

Bacteriophage Lambda Stabilization by Auxiliary Protein gpD: Timing, Location, and Mechanism of Attachment Determined by Cryo-EM

Gabriel C. Lander,^{1,2} Alex Evilevitch,³ Meerim Jeembaeva,³ Clinton S. Potter,¹ Bridget Carragher,¹ and John E. Johnson^{2,*}

¹National Resource for Automated Molecular Microscopy

²Department of Molecular Biology

The Scripps Research Institute, La Jolla, CA 92037, USA

³Department of Biochemistry, Center for Chemistry and Chemical Engineering, Lund University, S-221 33 Lund, Sweden

*Correspondence: jackj@scripps.edu

DOI 10.1016/j.str.2008.05.016

SUMMARY

We report the cryo-EM structure of bacteriophage lambda and the mechanism for stabilizing the 20-Å-thick capsid containing the dsDNA genome. The crystal structure of the HK97 bacteriophage capsid fits most of the $T = 7$ lambda particle density with only minor adjustment. A prominent surface feature at the 3-fold axes corresponds to the cementing protein gpD, which is necessary for stabilization of the capsid shell. Its position coincides with the location of the covalent cross-link formed in the docked HK97 crystal structure, suggesting an evolutionary replacement of this gene product in lambda by autocatalytic chemistry in HK97. The crystal structure of the trimeric gpD, in which the 14 N-terminal residues required for capsid binding are disordered, fits precisely into the corresponding EM density. The N-terminal residues of gpD are well ordered in the cryo-EM density, adding a strand to a beta-sheet formed by the capsid proteins and explaining the mechanism of particle stabilization.

INTRODUCTION

Bacteriophages, estimated to number on the order of 10^{31} on earth, are more abundant than any other organism within the biosphere (Wommack and Colwell, 2000). Over the last decade, a great surge of focused phage study, enabled by a marriage of genetic and structural methods, has provided a greatly improved understanding of their evolutionary relationships and structural mechanisms. Study of the *Escherichia coli*-infecting temperate bacteriophage lambda has helped shape the field of molecular biology, being used as a cloning vector and in the development of novel methods for in vitro packaging (Black, 1989; Chauthaiwale et al., 1992; Young and Davis, 1983). The virion consists of 405 copies of a capsid protein, gpE, arranged in an icosahedral shell with a $T = 7$ triangulation number. During prohead assembly, an oligomer made up of 12 copies of the portal protein, gpB, interacts with gpC to occupy one pentameric vertex of the head (Murialdo and Becker, 1978). Completion of

procapsid assembly results in a structural substrate for binding of the packaging machinery, and 48.5 kbp of double-stranded DNA (dsDNA) is pumped into the capsid chamber. Packaging of the lambda genome triggers a dramatic reconfiguration of the gpE proteins, and the capsid shell expands from roughly 50 nm in diameter to 60 nm while the capsid thickness decreases (Dokland and Murialdo, 1993). Concurrent with capsid expansion is a build-up of internal pressure within the shell, reaching upward of 60 atmospheres (Evilevitch et al., 2003; Fuller et al., 2007; Smith et al., 2001). To strengthen the capsid shell against the internal pressure of DNA packaging, a cementing protein, gpD, attaches to the quasi and icosahedral 3-fold vertices during expansion, stabilizing the mature phage capsid shell (Yang et al., 2000). The first 3-dimensional reconstructions of lambda accomplished using cryo-EM to 34 Å resolution by Dokland in 1993, revealed that the protruding gpD cementing proteins were distinguishable from the capsid proteins (Dokland and Murialdo, 1993). The cementing protein was crystallized, and an accompanying cryo-EM reconstruction at 15 Å resolution verified the crystal structure's orientation relative to the capsid (Yang et al., 2000). The first 14 residues of the gpD crystal structure, however, which were previously shown to be crucial for binding of gpD to the capsid shell, were disordered, such that a detailed description of the gpD-gpE interactions was impossible. Submission of the gpD primary sequence to the protein disorder prediction server (Ishida and Kinoshita, 2007) revealed that these N-terminal residues has a disorder probability of greater than 50%, and after this point in the sequence the disorder probability drops significantly. An NMR solution structure of the monomeric form of gpD confirmed the flexibility of these 14 residues (Iwai et al., 2005).

Here, we used electron cryo-microscopy (cryo-EM) and image reconstruction to examine the mature, icosahedrally averaged virion structure at subnanometer resolution. Individual polypeptide chains were clearly visible in regions of the density, and the details of gpD-capsid interaction and stabilization were determined. Comparison of the HK97 capsid protein crystal structure to the lambda capsid subunit reveals a striking similarity, and the HK97 crystal structure was used as a model for the gpE capsid protein. The N terminus of gpD is clearly visible as a single extended polypeptide chain that contributes an additional strand to a beta sheet formed by the capsid shell. We hypothesize that a network of these 4-stranded beta sheets formed by the binding of gpD creates a very stable capsid that copes with

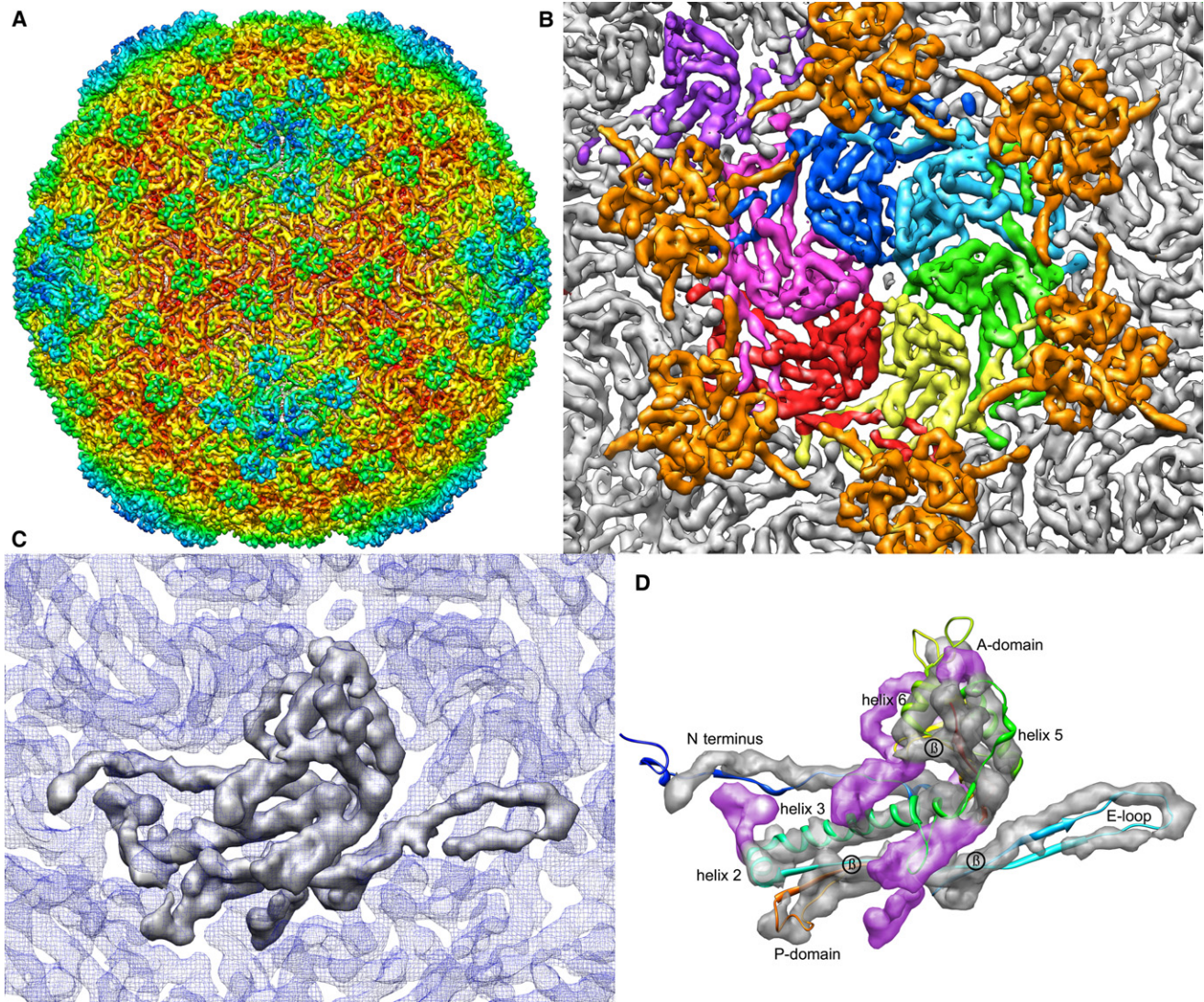


Figure 1. Three-Dimensional Density of Mature Bacteriophage Lambda Reconstructed from Cryo-EM Micrographs and Segmentation of a Single Monomer

(A) The subnanometer-resolution map of bacteriophage lambda colored radially from the phage center (red to blue). The reconstruction shows the $T = 7$ *laevo* symmetry of the capsid, and the decoration protein gpD as protruding densities at the quasi 3- and 6-fold vertices.

(B) A close-up, segmented view of the seven subunits that make up the icosahedral asymmetric unit, colored by subunit. The pentameric subunit is seen in the upper left-hand corner in purple. Surrounding the asymmetric unit are six gpD molecules, colored orange.

(C) One capsid subunit is shown as a surface representation in gray, in the context of the surrounding density, in blue mesh.

(D) Rigid-body fitting of HK97 crystal structure into the lambda monomer density, demonstrating closely similar morphology. For this fitting, the A domain of HK97 (residues 242–332 and 373–383) was separated from the rest of the crystal structure and fit independently, rotated 15° clockwise relative to HK97. Salient features observed in this map include homologous densities for helices 2, 3, 5, and 6, as well as putative beta-sheet densities, labeled in the figure. Additional density unaccounted for by the HK97 crystal structure (colored in purple) can be attributed to the additional 59 residues the lambda gpE contains in comparison to HK97.

the pressures of DNA packaging. A lower-resolution structure of the prohead is also presented here, showing that gpD is absent from the immature phage and that the gpE protein must change both quaternary and tertiary structure during maturation.

RESULTS

Cryo-EM Reconstruction of Isometric Lambda Particles

Phage lambda particles have thin angular capsid shells filled with dsDNA, and long straight tails when imaged under cryogenic

conditions in the transmission electron microscope (see [Figure S1](#) available online). Sixty-fold icosahedral symmetry was applied during the reconstruction process in order to maximize the signal-to-noise ratio of the raw data, allowing for subnanometer resolution of the structure. [Figure 1A](#) shows the resulting icosahedrally averaged lambda capsid structure, at a resolution of 6.8 Å according to rmeasure 0.5 criterion ([Harauz and Van Heel, 1986](#); [Sousa and Grigorieff, 2007](#)) (7.7 Å by the FSC 0.5 criteria), although disordered DNA within the capsid interior may be negatively affecting these resolution calculations. Detail

observed in the density support the 6.8 Å estimate. The overall size and morphology of the capsid is consistent with previously observed structures calculated at lower resolutions. The average diameter of the particle is ~600 Å, exhibiting T = 71 symmetry with protruding densities corresponding to gpD at the icosahedral and quasi 3-fold axes.

Lambda and HK97, both members of the lambdoid family, have very similar dimensions when their central slices are compared, except along the 3-fold axis, where the phage lambda capsid density diameter protrudes an additional 75 Å due to the attachment of gene product D to the capsid shell (Figure S2). Additionally, since the lambda density was reconstructed from fully packaged wild-type virions, the concentrically packed dsDNA is clearly visible within the lambda capsid interior, condensed with a spacing of roughly 24 Å from one DNA strand center to the next. On the basis of the crystal structure of HK97, the interior of the lambda capsid likely carries a negative overall charge, which explains why the DNA does not directly contact the capsid wall.

The reconstructed lambda EM density was at sufficient resolution to delineate intersubunit boundaries within the icosahedral subunit, allowing for segmentation of the seven independent asymmetric subunits (Figure 1B). The close structural similarity between the segmented subunits is indicative of the high quality of the reconstructed map. Not surprisingly, in spite of a complete lack of primary sequence homology, the HK97 fold is clearly evident (Figures 1C and 1D), as was previously observed in many other dsDNA icosahedral phage (Agirrezabala et al., 2007; Baker et al., 2005; Fokine et al., 2005; Jiang et al., 2003, 2006, 2008; Morais et al., 2005; Wikoff et al., 2000). The signature helix 3 is unmistakable, with a length of ~40 Å, along with a shorter rod of density continuing from this structure that may correspond to helix 2. Helices 5 and 6 (25 and 15 Å long, respectively) are seen in domain A, and a large flat density, probably corresponding to the antiparallel sheets, are below the helices located at the center of the HK97 wedge. Additional secondary structure similarities include the P Domain, with the appearance of antiparallel beta sheets, and the long E-loop extending toward the icosahedral and quasi 3-fold axes. The extended N-terminal arm is clearly visible reaching out from the body of the subunit in a clockwise direction and interacting with the E-loop strand of the neighboring subunit. The N terminus of HK97 is known to be involved in an acrobatic quaternary interaction (Wikoff et al., 2000), and the density presented here shows that the lambda N terminus is involved in similar associations; it spans the quasi 2-fold axis, contacting two other asymmetric subunits in the process. Having accounted for these structural similarities, there remains a significant region of density in the lambda reconstruction for which there is no HK97 counterpart arising from the additional 59 residues present in lambda gpE (Figure 1D). Nevertheless, it is clear that the two phages share a common fold and that major secondary structural elements in HK97 have homology in lambda.

Cementing Protein gpD

The largest morphological difference between the lambda and HK97 capsid structures is the additional gene product, gpD, bound to lambda's capsid surface. The gpD trimer was shown to stabilize the capsid shell during DNA packaging, and mutants missing this essential gene product can package little more than

80% of its genome (Sternberg and Weisberg, 1977). Upon maturation, conformational changes of the capsid structure either expose or form new binding sites for the attachment of gpD at the quasi and icosahedral 3-folds. First visualized in complex with the capsid at 34 Å resolution as "thimble-shaped" protrusions at the 3-fold axes, gpD was interpreted to bind as a trimer (Dokland and Murialdo, 1993). This was confirmed by the crystallization of gpD as a trimer and its accommodation into a 15 Å cryo-EM reconstruction (Yang et al., 2000). The cryo-EM reconstruction determined the gpD trimer orientation, showing that both the N and C termini come into close proximity of the capsid surface. The first 14 residues of gpD, which were shown to be crucial for proper binding of gpD to the capsid (Wendt and Feiss, 2004; Yang et al., 2000), were disordered in the crystal structure, suggesting an ordering of the N termini upon interaction with the gpE capsid protein. Without the structured N termini, no further information regarding the gpD-gpE interaction was attainable from the previous 15 Å EM reconstruction.

When docked into its location on the capsid surface of the higher resolution map described here, the trimeric crystal structure of gpD (Yang et al., 2000) exhibits exceptionally high correlation with the lambda cryo-EM density (Figure 2A). Since gpD is necessary for lambda stabilization during DNA packaging and HK97 lacks this gene product, we propose that the maturation-dependent cross-link in HK97 is related to the role played by gpD to lambda. When the refined HK97 crystal structure (Helgstrand et al., 2003) was docked into the lambda reconstruction, the location of HK97's lysine 169 and asparagine 356 residues, involved in cross-linking different subunits, were directly under the individual gpD monomers (Figures 3A and 3B). Thus, the location of cross-links in HK97 and the gpD binding position in lambda are superimposed.

The lambda subnanometer map allowed specific features of the gpD binding site to be observed that were not discernable in previous studies. Although the N termini in the crystal structure of isolated gpD are completely disordered, in the cryo-EM map we see well-ordered density extending from the N terminus of the docked gpD crystal structure that connects the gpD density to the lambda capsid surface. This density supports the proposal by Yang et al. (2000) that the N terminus becomes ordered when gpD binds to the capsid. This N-terminal density was modeled with coordinates for an extended polypeptide of 14 amino acids and was found to extend away from the gpD of origin, interacting with a strand of the E-loop of the capsid protein (Figure 2B). Although the resolution of the EM map is not sufficient to distinguish individual side chains, this extended density convincingly accommodates a 14-residue polypeptide chain. The last residues of gpD N terminus are involved in a 4-stranded beta sheet, with the other three strands coming from the subunit's E-loop and a neighboring subunit's N terminus (Figure 2B). Secondary structure prediction based on the gpD sequence is consistent with beta structure in the N-terminal region (Figure S3). The creation of this 4-stranded beta sheet generates a strong interaction between gpD and gpE, and the trimeric nature of the bound gpD fastens six subunits from three different capsomers together in a manner remarkably similar to the cross-links in HK97. It is likely that the overall surface charge topography of gpD, which has a hydrophilic surface that faces away from the lambda capsid and a hydrophobic surface that is sequestered from solvent

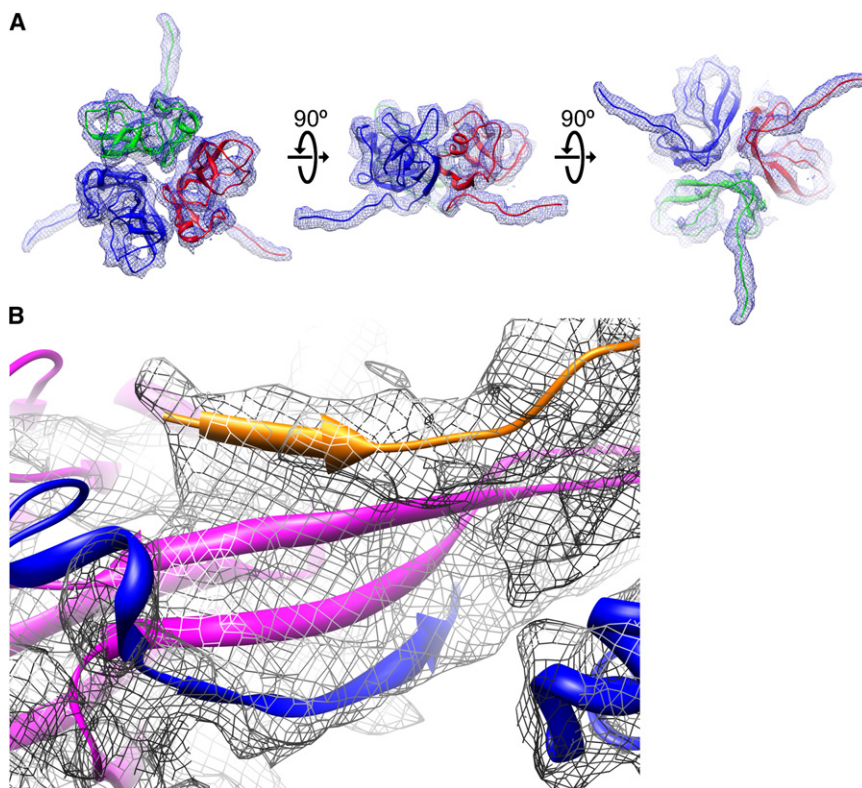


Figure 2. Density Corresponding to gpD, with Modeled N-Terminal Residues

(A) Top, side, and bottom views of gpD are displayed with the 1.1 Å crystal structure (PDB ID: 1C5E) fit into the reconstructed EM density, colored by subunit. Polyalanine peptides of the 14 disordered residues of the N terminus were modeled into the density, which can be seen extending away from the main body of the gpD trimer. It is evident from these views why the N terminus is disordered in the absence of the mature capsid substrate.

(B) The stabilizing 4-stranded beta sheet. During maturation of phage lambda, the E-loop of one gpE capsid protein (magenta) interacts with the N terminus of a neighboring gpE subunit within the same capsomer (blue), forming a beta sheet similar to that seen in HK97. Although the individual polypeptide strands that make up the beta sheet are not distinguishable in the EM density, this density accommodates the HK97 3-stranded beta sheet. An additional strand is contributed by gpD (orange) as it binds to the capsid surface, shown by the contribution of an additional density above the three capsid strands.

when bound, drives the initial binding of gpD to the capsid, and that the gpD-gpE interaction is enhanced by the resulting beta sheet structures.

Reconstruction of Lambda Prohead Particles

Cryo-EM micrographs of a lambda packaging mutant preparation exhibited numerous prohead particles (Figure S4). Prohead particles lack DNA and tails and have not undergone the conformational expansion associated with maturation. Compared with mature phage, they have a thicker capsid wall, smaller diameter, and a rounded, less angular morphology. Prohead particles lack the gpD protein, since the binding site is exposed upon particle expansion. To determine whether this is the case, a 3-dimensional density was reconstructed with these particles to a resolution between 13.3 Å and 14.5 Å (according to FSC 0.5 and rmeasure 0.5 criteria, respectively). The overall morphology of the prohead agrees with previous reconstructions (Dokland and Murialdo, 1993), although the higher resolution allows for a clear delineation of each subunit making up the hexameric and pentameric capsomers and delineation of the subunit domains (Figure 4C).

Comparison with mature phage shows that a dramatic rearrangement of the capsid architecture occurs during maturation. Maturation was first documented by EM in 1976 using T4 polyheads (Laemmli et al., 1976), and since then it has been described at various resolutions in a number of other dsDNA bacteriophage (Conway et al., 2001; Dokland and Murialdo, 1993; Gan et al., 2006; Jiang et al., 2003; Wang et al., 2003). Regardless of the phage analyzed, there are common structural differences between prophage capsids and mature capsids. Prophage shells are thick (~40Å), round, and relatively small (~500 Å in diameter) with “hexameric” capsomers that are

skewed and not 6-fold symmetric. Mature phage shells are thin (~20 Å), icosahedral-shaped and about 650 Å in diameter with 6-fold symmetric hexamer capsomers. While lambda undergoes these changes during maturation, it is novel when compared to P22 and HK97, in that a binding site for the gpD protein is created during maturation.

Recently, an *E. coli* gene encoding for a putative capsid protein of a prophage was crystallized (R. Zhang, C Hatzos, J. Abdullah, and A. Joachimiak, personal communication) displaying a domain structure strikingly similar to that of the HK97 fold, but with obvious differences in the disposition of tertiary structure domains. The sequence of the prophage capsid protein is 43% identical to the phage capsid protein, and the crystal structure fits into the lambda procapsid EM density with high fidelity (Figure 4B). Examination of the procapsid quasi and icosahedral 3-fold regions in the context of the atomic model reveals that the regions that interact with the main body of the gpD trimer in the mature phage are interior in the procapsid shell and inaccessible for gpD binding. Residues in the E-loops of the prophage subunit crystal structure have the highest temperature factors in the crystal and are probably held in place by crystal contacts. There is no EM density corresponding to the E loops in the reconstruction, indicating that they are dynamic in the lambda procapsid particle. The mature phage reconstruction has the N terminus of gpD bound to a strand of the E-loop of gpE stabilizing it and its interactions with neighboring capsid regions.

DISCUSSION

The lambda phage cryo-EM map presented here enables us to see a single polypeptide interacting with an existing beta sheet

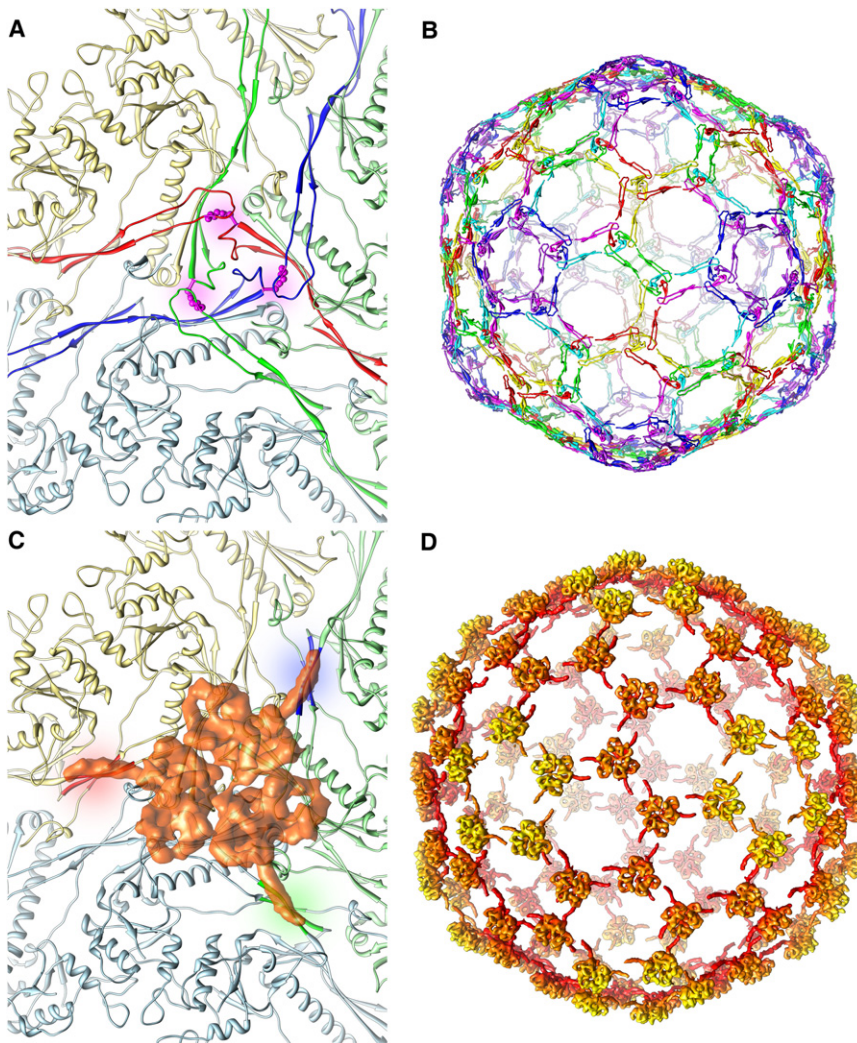


Figure 3. Homologous Stabilization Method in Lambda and HK97

A 3-fold vertex of the HK97 crystal structure is shown as a ribbon, each capsomer colored differently (light blue, yellow, and green).

(A) The HK97 lysine-asparagine cross-link, colored in magenta, secure the three capsomers covalently, such that a cementing protein is not necessary. The polypeptide arms involved in creation of the HK97 chain mail are colored in red, blue, and green.

(B) The regions of HK97 that are involved with formation of the chain mail. A clear similarity to lambda can be observed, with the gpD monomers assembled at the quasi and icosahedral 3-fold vertices, while in HK97, the covalent cross-links are formed at precisely corresponding regions.

(C) Density from the reconstruction corresponding to gpD has been overlaid semitransparently as it is situated in lambda. Note that although lambda does not undergo covalent cross-link formation, gpD's N-terminal arms form strong beta-sheet interactions with each of three capsomers, securing the capsid at the 3-fold. Sites of interaction are colored in red, blue, and green.

(D) All the icosahedrally related gpD proteins as they bind to the surface of lambda, revealing a network of interactions that are similar to those seen in HK97. The N terminus of lambda extends along a similar trajectory as that of HK97's E-loops, effectively stitching capsomers together in a homologous manner.

It is clear that the molecular architecture of HK97 and lambda are closely related, with the major exception being a gene that encodes the stabilization protein gpD in lambda. A means by which to stabilize the mature capsid against extremes in pH and temperature as well as

on the surface of the lambda capsid. The observed interactions explain the role of gpD in capsid stabilization during DNA packaging, leading to an interpretation of the evolutionary pathway followed by lambda, HK97, and many other phages with similar subunit folds. The genomes of over a dozen different members of the lambdoid family have been sequenced, revealing very similar genetic maps with the head genes clustered at the left end in a stereotypical order: terminase, portal, protease, scaffolding, and capsid protein (Casjens, 2005; Juhala et al., 2000; Lawrence et al., 2002). It is surprising to find that in phages whose genomes share only faint hints of sequence similarity, an obvious similarity in the ordering of the genes persists (Campbell, 1994; Casjens, 2005). The shared genetic structure between these phages provides evidence for a common ancestry. Subunit structures, however, show that ancestral relationships extend further than expected, to phages that were previously thought to have completely diverged along separate lineages. The medium-to-high resolution structures of various lambdoid phages exhibit capsid folds that are strikingly similar (Agirrezabala et al., 2007; Fokine et al., 2005; Jiang et al., 2003, 2006; Wikoff et al., 2000), a characteristic that extends even to phages outside of the lambdoid family (Baker et al., 2005; Morais et al., 2005).

other factors in their hostile environment is a presumed necessity accomplished by all phages. Mechanical stability of the thin mature coat shell is also required to withstand the pressures resulting from packaging of DNA to liquid crystalline densities. Fuller et al. (2007) have shown that packaging of DNA into lambda phages in the absence of gpD sometimes leads to a rupture of the capsid shell.

HK97 undergoes a conformational change during expansion that brings a lysine residue into close proximity of a neighboring subunit's asparagines, ligating the two subunits together with a chemical linkage. The icosahedral symmetry of these chemical linkages results in the creation of an elaborate and robust chain mail shroud that surrounds the packaged DNA (Wikoff et al., 2000). Lacking the chemical linkages, lambda utilizes gpD for capsid stabilization, a phenomenon not unique to this phage. Phage T4, phage L, phage phi29, adenovirus, and herpesvirus are all examples of dsDNA viruses that embellish their mature capsid structures with such stabilization proteins (Fokine et al., 2004; Furcinitti et al., 1989; Ishii and Yanagida, 1977; Iwasaki et al., 2000; Morais et al., 2005; Saad et al., 1999; Schrag et al., 1989; Steven et al., 1992; Stewart et al., 1991; Tang et al., 2006; Tao et al., 1998; Trus et al., 1996). Interestingly, T4, whose Hoc

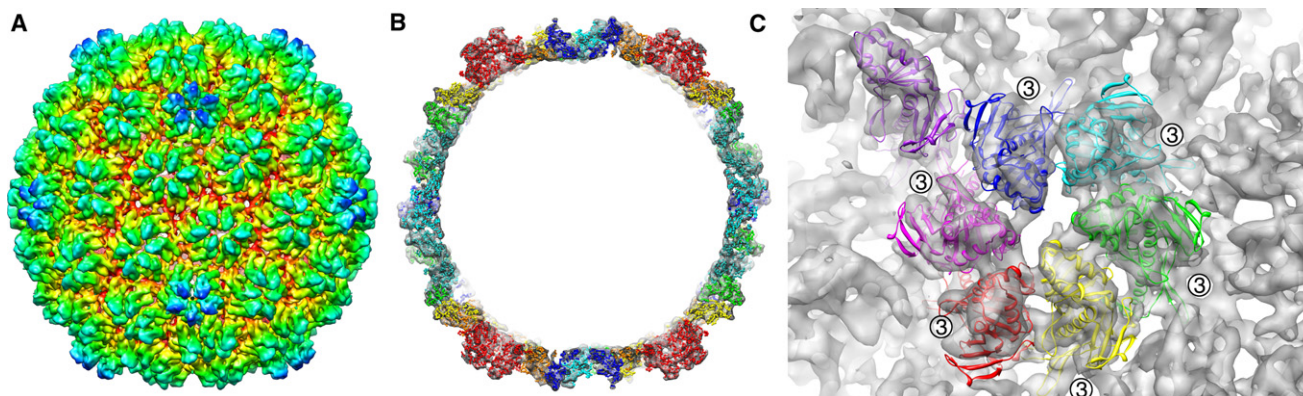


Figure 4. Three-Dimensional Density of the Procapsid Form of Bacteriophage Lambda

(A) Radially colored surface representation of the cryo-EM reconstruction of the lambda procapsid. $T = 71$ symmetry is evident, along with the skewed hexamers seen in many phage procapsids.

(B) Cross-section view of the EM procapsid density, with the atomic coordinates of a related lambdoid phage modeled into the icosahedral shell. The atomic model docked into position is homologous in length to lambda, and accounts for virtually all the density of the procapsid. Because there are no large densities that do not have a corresponding procapsid model, we can be sure that the gpE trimer is not bound to the procapsid state.

(C) A pseudo-atomic model of the procapsid asymmetric unit, with the quasi and icosahedral 3-fold vertices labeled. Here, we see the immature binding site of gpD before expansion. The 3-fold surfaces are buried deep within the folds of the thick procapsid shell, preventing attachment of the gpD monomers, and the E-loop, with which the N terminus of gpD forms a beta sheet, is disordered and pointed away from the capsid surface.

and Soc were the first such stability-inducing proteins to be characterized (Ishii and Yanagida, 1977), has a 60-residue insertion where the E-loop hairpin of HK97 is located in the sequence. These domains are brought into association with symmetrically related subunits, implicating a similar role to the cross-links of HK97, an example of a phage that is stabilized via neighboring domain associations in addition to supplementary protein binding (Fokine et al., 2005). Since gpD was implicated through many studies to be necessary for capsid stabilization (Sternberg and Weisberg, 1977; Wendt and Feiss, 2004; Yang et al., 2000), we hypothesize that HK97 evolved to replace this stabilizing gene product by developing the chemistry to form intersubunit cross-links that form a chain mail-like structure, securing the mature head (Figure 3D).

When the lambda capsid protein is computationally removed from the EM reconstruction, leaving only the density corresponding to gpD, the arrangement of the N-terminal polypeptide involved in the stabilization of the capsid shell exhibits a striking analogy to the regions involved in HK97's covalent chain mail lattice (Figures 3C and 3D). These N-terminal arms stretch along a path that is laid out by the E-loops, forming a series of hexagons and pentagons that envelope the lambda capsid, integrated through 420 beta sheet interactions. In this manner, adjacent capsomers are united at each of the quasi and icosahedral 3-folds by the trimerization of the monomeric gpD subunits.

It has been proposed that gpD may have been inserted as a "moron" gene in an ancestral lambda genome, and preserved as a result of an increased fitness of the resulting phage by the stability of its capsid (Hendrix et al., 2000). In this vein, it is conceivable that lambda and HK97 may have both evolved from a single ancient genome where the accidental incorporation of an auxiliary gene resulted in an increased fitness, thus sending the resultant phage down an evolutionary branch of increased fitness, while a separate divergence accomplished the same effect via elegant chemistry. The fact that the stabilization point

in both of these phages is localized to the trigonally symmetric sites might be construed as convergent evolution, but it is also possible that this aspect is evidence of divergent evolution. It can be argued that the ancestral genomes of both HK97 and lambda included this cementing protein and that HK97 did away with the need for this auxiliary gene product by evolving clever chemistry.

The case for gpD playing a homologous role as HK97's cross-links is further supported by the similarity of the lambda procapsid reconstruction to the HK97 procapsid (Conway et al., 2001). Cross-links occur as subunits move from a roughly radial direction in their elongated dimension to a roughly tangential orientation, bringing the E-loops and P-domains of neighboring subunits into close proximity to each other. During capsid expansion, the corresponding domains in lambda are similarly brought together, creating a binding site for gpD, which in turn stabilizes the shell without covalent linkages. The stage for the cross-linking phenomena has, however, been set by lambda's gpD. The domains necessary for cross-link formation are in close proximity in lambda, and given the rate of mutation seen in these phages, it would only be a matter of time before mutation of two residues would do away with the necessity for this auxiliary gene product.

EXPERIMENTAL PROCEDURES

Production and Purification of Lambda Virions

Wild-type bacteriophage lambda with genome length 48.5 kbp was produced by thermal induction of lysogenic *E. coli* strain AE1. The AE1 strain was modified to grow without LamB protein expressed on its surface in order to increase the yield of phage induced in the cell. The culture was then lysed by temperature induction. Phage was purified by CsCl equilibrium centrifugation. The sample was dialyzed from CsCl against TM buffer (10 mM $MgSO_4$ and 50 mM Tris-HCl [pH 7.4]). The final titer was 10^{13} virions/ml, determined by plaque assay. Phage purification details have been described elsewhere (Evelitch et al., 2003).

The prohead particles appeared in a preparation of the mutant phage lambda b221c126, which packages a 37.7 kbp genome. Purification details have been described elsewhere (Grayson et al., 2006).

Electron Microscopy

Lambda phages were prepared for cryo-EM analysis by preservation in vitreous ice over a holey carbon substrate via rapid-freeze plunging. The holey carbon films used were developed at NRAMM and are currently commercially available from Protochips Inc. under the name Cflats. They consist of 400-mesh copper grids onto which a layer of pure carbon fenestrated by 2 μm holes spaced 4 μm apart was applied. Grids were cleaned before freezing by use of a plasma cleaner (Fischione Instruments, Inc.) using 75% argon and 25% oxygen for 25 sec. A 3 μl aliquot of sample was applied to the grids, which were loaded into an FEI Vitrobot (FEI company) with settings at 4°C, 100% humidity, and a blot offset of -2 . The grids were double-blotted for 7 sec at a time and immediately plunged into liquid ethane. Grids were stored in liquid nitrogen until being loaded into the microscope for data collection.

Data Collection

Mature Virion

Data were acquired using a Tecnai F20 Twin transmission electron microscope, operating at 200 keV at liquid nitrogen temperatures and equipped with a Tietz F415 4k \times 4k pixel CCD camera (15 μm pixel) and a Gatan side entry cryostage. Six data sets were collected from six different grids at a nominal magnification of 80,000 \times with a pixel size of 1.01 \AA . A total of 2471, 788, 2090, 770, 686, and 1939 images were recorded during the six sessions using the Leginon automated electron microscopy package (Suloway et al., 2005) with a randomized defocus range from $-0.8 \mu\text{m}$ to $-2.5 \mu\text{m}$ at a dose of $19 \text{ e}^{-}/\text{\AA}^2$. Concurrent with data collection, preliminary image analysis was performed with the use of a new software package, Appion, which is currently under development at NRAMM. Automated particle picking (Roseman, 2003) and automated CTF estimation (Mallick et al., 2005) were performed on each image as it was collected.

Procapsids

Data were acquired on the same model of microscope running under the same conditions as above, but outfitted with a Gatan 4k \times 4k CCD (Gatan Inc), at a nominal magnification of 50,000 \times , with a pixel size of 2.26 \AA . A total of 2683 images were collected, which were processed in the same manner as the above.

Single Particle Reconstruction

Mature Virion

Initial particle selection by automated methods was inspected manually with an Appion module, yielding 5565, 1932, 7811, 7550, 4653, and 14344 particles from each of the six data collection sessions. Particles were extracted from the images whose CTF estimation had a confidence of 80% or higher using a box size of 768 pixels on an edge. The phases of the images were corrected according to the CTF estimation during creation of the stack, and the particles were centered using functions included in the EMAN software package (Ludtke et al., 1999). The resulting 31,422-particle stack was binned by a factor of two for reconstruction by EMAN, using an icosahedrally averaged reconstruction of bacteriophage P22 (Lander et al., 2006), low-pass filtered to 40 \AA as the starting model. Particles iterated through 20 rounds of refinement, beginning at an angular increment of 5° and decreased by 1° at four iteration intervals. An additional four rounds of refinement were then performed at an angular increment of 0.5°, the last round of which provided the density reported. The amplitudes of the resulting refined structure were adjusted with the SPIDER software package (Frank et al., 1996) to fit the density Fourier amplitudes to an experimental 1D low-angle X-ray scattering curve.

Procapsids

Processing was performed in the same manner as for the mature virion, using 4640 particle images with a box size of 384 pixels. The EMAN function "starticos" was used to create an initial model. Particles were not manually inspected as in the mature virion reconstruction, nor were the last four iterations of refinement at an angular increment of 0.5° performed.

Rigid-body docking of crystal structures into the cryo-EM density and graphical representations were produced with the Chimera visualization software package (Goddard et al., 2007). The 14-residue N-terminal polypeptide

of gpD was modeled as a polyaniline chain into the EM density with the Coot crystallography package (Emsley and Cowtan, 2004).

ACCESSION NUMBERS

Density maps of the mature and prophage forms of phage lambda have been deposited at the Electron Microscopy Data Bank (EMDB) under reference numbers EMD-5012 and EMD-1507, respectively.

SUPPLEMENTAL DATA

Supplemental data include three figures and Supplemental References and can be found with this article online at <http://www.structure.org/cgi/content/full/16/9/1399/DC1/>.

ACKNOWLEDGMENTS

We thank William Young for providing extensive computational support throughout the reconstruction processes. We are also grateful to Alan Davidson for stimulating discussions regarding capsid maturation. Electron microscopic imaging and reconstruction was conducted at the National Resource for Automated Molecular Microscopy, which is supported by the National Institutes of Health (NIH) through the National Center for Research Resources' P41 program (grant RR17573). This work was also supported by grants from the Swedish Research Council and Royal Physiographic Society (to A.E.), by NIH (grant R01 GM054076 to J.E.J.), and a fellowship from the ARCS foundation (to G.C.L.).

Received: April 15, 2008

Revised: May 23, 2008

Accepted: May 28, 2008

Published: September 9, 2008

REFERENCES

- Agirrezabala, X., Velazquez-Muriel, J.A., Gomez-Puertas, P., Scheres, S.H., Carazo, J.M., and Carrascosa, J.L. (2007). Quasi-atomic model of bacteriophage T7 procapsid shell: insights into the structure and evolution of a basic fold. *Structure* 15, 461–472.
- Baker, M.L., Jiang, W., Rixon, F.J., and Chiu, W. (2005). Common ancestry of herpesviruses and tailed DNA bacteriophages. *J. Virol.* 79, 14967–14970.
- Black, L.W. (1989). DNA packaging in dsDNA bacteriophages. *Annu. Rev. Microbiol.* 43, 267–292.
- Campbell, A. (1994). Comparative molecular biology of lambdoid phages. *Annu. Rev. Microbiol.* 48, 193–222.
- Casjens, S.R. (2005). Comparative genomics and evolution of the tailed-bacteriophages. *Curr. Opin. Microbiol.* 8, 451–458.
- Chauthaiwale, V.M., Therwath, A., and Deshpande, V.V. (1992). Bacteriophage lambda as a cloning vector. *Microbiol. Rev.* 56, 577–591.
- Conway, J.F., Wikoff, W.R., Cheng, N., Duda, R.L., Hendrix, R.W., Johnson, J.E., and Steven, A.C. (2001). Virus maturation involving large subunit rotations and local refolding. *Science* 292, 744–748.
- Dokland, T., and Murialdo, H. (1993). Structural transitions during maturation of bacteriophage lambda capsids. *J. Mol. Biol.* 233, 682–694.
- Emsley, P., and Cowtan, K. (2004). Coot: model-building tools for molecular graphics. *Acta Crystallogr. D Biol. Crystallogr.* 60, 2126–2132.
- Evilevitch, A., Lavelle, L., Knobler, C.M., Raspaud, E., and Gelbart, W.M. (2003). Osmotic pressure inhibition of DNA ejection from phage. *Proc. Natl. Acad. Sci. USA* 100, 9292–9295.
- Fokine, A., Chipman, P.R., Leiman, P.G., Mesyanzhinov, V.V., Rao, V.B., and Rossmann, M.G. (2004). Molecular architecture of the prolate head of bacteriophage T4. *Proc. Natl. Acad. Sci. USA* 101, 6003–6008.
- Fokine, A., Leiman, P.G., Shneider, M.M., Ahvazi, B., Boeshans, K.M., Steven, A.C., Black, L.W., Mesyanzhinov, V.V., and Rossmann, M.G. (2005). Structural and functional similarities between the capsid proteins of bacteriophages T4

- and HK97 point to a common ancestry. *Proc. Natl. Acad. Sci. USA* **102**, 7163–7168.
- Frank, J., Radermacher, M., Penczek, P., Zhu, J., Li, Y., Ladjadj, M., and Leith, A. (1996). SPIDER and WEB: processing and visualization of images in 3D electron microscopy and related fields. *J. Struct. Biol.* **116**, 190–199.
- Fuller, D.N., Raymer, D.M., Rickgauer, J.P., Robertson, R.M., Catalano, C.E., Anderson, D.L., Grimes, S., and Smith, D.E. (2007). Measurements of single DNA molecule packaging dynamics in bacteriophage lambda reveal high forces, high motor processivity, and capsid transformations. *J. Mol. Biol.* **373**, 1113–1122.
- Furcinitti, P.S., van Oostrum, J., and Burnett, R.M. (1989). Adenovirus polypeptide IX revealed as capsid cement by difference images from electron microscopy and crystallography. *EMBO J.* **8**, 3563–3570.
- Gan, L., Speir, J.A., Conway, J.F., Lander, G., Cheng, N., Firek, B.A., Hendrix, R.W., Duda, R.L., Liljas, L., and Johnson, J.E. (2006). Capsid conformational sampling in HK97 maturation visualized by X-ray crystallography and cryo-EM. *Structure* **14**, 1655–1665.
- Goddard, T.D., Huang, C.C., and Ferrin, T.E. (2007). Visualizing density maps with UCSF Chimera. *J. Struct. Biol.* **157**, 281–287.
- Grayson, P., Evilevitch, A., Inamdar, M.M., Purohit, P.K., Gelbart, W.M., Knobler, C.M., and Phillips, R. (2006). The effect of genome length on ejection forces in bacteriophage lambda. *Virology* **348**, 430–436.
- Harauz, G., and Van Heel, M. (1986). Exact filters for general geometry three dimensional reconstruction. *Optik* **73**, 146–156.
- Helgstrand, C., Wikoff, W.R., Duda, R.L., Hendrix, R.W., Johnson, J.E., and Liljas, L. (2003). The refined structure of a protein catenane: the HK97 bacteriophage capsid at 3.44 Å resolution. *J. Mol. Biol.* **334**, 885–899.
- Hendrix, R.W., Lawrence, J.G., Hatfull, G.F., and Casjens, S. (2000). The origins and ongoing evolution of viruses. *Trends Microbiol.* **8**, 504–508.
- Ishida, T., and Kinoshita, K. (2007). PrDOS: prediction of disordered protein regions from amino acid sequence. *Nucleic Acids Res.* **35**, W460–W464.
- Ishii, T., and Yanagida, M. (1977). The two dispensable structural proteins (soc and hoc) of the T4 phage capsid; their purification and properties, isolation and characterization of the defective mutants, and their binding with the defective heads in vitro. *J. Mol. Biol.* **109**, 487–514.
- Iwai, H., Forrer, P., Pluckthun, A., and Guntert, P. (2005). NMR solution structure of the monomeric form of the bacteriophage lambda capsid stabilizing protein gpD. *J. Biomol. NMR* **31**, 351–356.
- Iwasaki, K., Trus, B.L., Wingfield, P.T., Cheng, N., Campusano, G., Rao, V.B., and Steven, A.C. (2000). Molecular architecture of bacteriophage T4 capsid: vertex structure and bimodal binding of the stabilizing accessory protein. *Soc. Virology* **271**, 321–333.
- Jiang, W., Li, Z., Zhang, Z., Baker, M.L., Prevelige, P.E., Jr., and Chiu, W. (2003). Coat protein fold and maturation transition of bacteriophage P22 seen at subnanometer resolutions. *Nat. Struct. Biol.* **10**, 131–135.
- Jiang, W., Chang, J., Jakana, J., Weigele, P., King, J., and Chiu, W. (2006). Structure of epsilon15 bacteriophage reveals genome organization and DNA packaging/injection apparatus. *Nature* **439**, 612–616.
- Jiang, W., Baker, M.L., Jakana, J., Weigele, P.R., King, J., and Chiu, W. (2008). Backbone structure of the infectious epsilon15 virus capsid revealed by electron cryomicroscopy. *Nature* **451**, 1130–1134.
- Juhala, R.J., Ford, M.E., Duda, R.L., Youlton, A., Hatfull, G.F., and Hendrix, R.W. (2000). Genomic sequences of bacteriophages HK97 and HK022: pervasive genetic mosaicism in the lambdoid bacteriophages. *J. Mol. Biol.* **299**, 27–51.
- Laemmli, U.K., Amos, L.A., and Klug, A. (1976). Correlation between structural transformation and cleavage of the major head protein of T4 bacteriophage. *Cell* **7**, 191–203.
- Lander, G.C., Tang, L., Casjens, S.R., Gilcrease, E.B., Prevelige, P., Poliakov, A., Potter, C.S., Carragher, B., and Johnson, J.E. (2006). The structure of an infectious P22 virion shows the signal for headful DNA packaging. *Science* **312**, 1791–1795.
- Lawrence, J.G., Hatfull, G.F., and Hendrix, R.W. (2002). Imbroglis of viral taxonomy: genetic exchange and failings of phenetic approaches. *J. Bacteriol.* **184**, 4891–4905.
- Ludtke, S.J., Baldwin, P.R., and Chiu, W. (1999). EMAN: semiautomated software for high-resolution single-particle reconstructions. *J. Struct. Biol.* **128**, 82–97.
- Mallick, S.P., Carragher, B., Potter, C.S., and Kriegman, D.J. (2005). ACE: automated CTF estimation. *Ultramicroscopy* **104**, 8–29.
- Morais, M.C., Choi, K.H., Koti, J.S., Chipman, P.R., Anderson, D.L., and Rossmann, M.G. (2005). Conservation of the capsid structure in tailed dsDNA bacteriophages: the pseudoatomic structure of phi29. *Mol. Cell* **18**, 149–159.
- Murialdo, H., and Becker, A. (1978). Head morphogenesis of complex double-stranded deoxyribonucleic acid bacteriophages. *Microbiol. Rev.* **42**, 529–576.
- Roseman, A.M. (2003). Particle finding in electron micrographs using a fast local correlation algorithm. *Ultramicroscopy* **94**, 225–236.
- Saad, A., Zhou, Z.H., Jakana, J., Chiu, W., and Rixon, F.J. (1999). Roles of triplex and scaffolding proteins in herpes simplex virus type 1 capsid formation suggested by structures of recombinant particles. *J. Virol.* **73**, 6821–6830.
- Schrag, J.D., Prasad, B.V., Rixon, F.J., and Chiu, W. (1989). Three-dimensional structure of the HSV1 nucleocapsid. *Cell* **56**, 651–660.
- Smith, D.E., Tans, S.J., Smith, S.B., Grimes, S., Anderson, D.L., and Bustamante, C. (2001). The bacteriophage straight phi29 portal motor can package DNA against a large internal force. *Nature* **413**, 748–752.
- Sousa, D., and Grigorieff, N. (2007). Ab initio resolution measurement for single particle structures. *J. Struct. Biol.* **157**, 201–210.
- Sternberg, N., and Weisberg, R. (1977). Packaging of coliphage lambda DNA. II. The role of the gene D protein. *J. Mol. Biol.* **117**, 733–759.
- Steven, A.C., Greenstone, H.L., Booy, F.P., Black, L.W., and Ross, P.D. (1992). Conformational changes of a viral capsid protein: thermodynamic rationale for proteolytic regulation of bacteriophage T4 capsid expansion, co-operativity, and super-stabilization by soc binding. *J. Mol. Biol.* **228**, 870–884.
- Stewart, P.L., Burnett, R.M., Cyrklaff, M., and Fuller, S.D. (1991). Image reconstruction reveals the complex molecular organization of adenovirus. *Cell* **67**, 145–154.
- Suloway, C., Pulokas, J., Fellmann, D., Cheng, A., Guerra, F., Quispe, J., Stagg, S., Potter, C.S., and Carragher, B. (2005). Automated molecular microscopy: the new Legimon system. *J. Struct. Biol.* **151**, 41–60.
- Tang, L., Gilcrease, E.B., Casjens, S.R., and Johnson, J.E. (2006). Highly discriminatory binding of capsid-cementing proteins in bacteriophage L. *Structure* **14**, 837–845.
- Tao, Y., Olson, N.H., Xu, W., Anderson, D.L., Rossmann, M.G., and Baker, T.S. (1998). Assembly of a tailed bacterial virus and its genome release studied in three dimensions. *Cell* **95**, 431–437.
- Trus, B.L., Booy, F.P., Newcomb, W.W., Brown, J.C., Homa, F.L., Thomsen, D.R., and Steven, A.C. (1996). The herpes simplex virus procapsid: structure, conformational changes upon maturation, and roles of the triplex proteins VP19c and VP23 in assembly. *J. Mol. Biol.* **263**, 447–462.
- Wang, S., Chandramouli, P., Butcher, S., and Dokland, T. (2003). Cleavage leads to expansion of bacteriophage P4 procapsids in vitro. *Virology* **314**, 1–8.
- Wendt, J.L., and Feiss, M. (2004). A fragile lattice: replacing bacteriophage lambda's head stability gene D with the shp gene of phage 21 generates the Mg2+-dependent virus, lambda shp. *Virology* **326**, 41–46.
- Wikoff, W.R., Liljas, L., Duda, R.L., Tsuruta, H., Hendrix, R.W., and Johnson, J.E. (2000). Topologically linked protein rings in the bacteriophage HK97 capsid. *Science* **289**, 2129–2133.
- Wommack, K.E., and Colwell, R.R. (2000). Virioplankton: viruses in aquatic ecosystems. *Microbiol. Mol. Biol. Rev.* **64**, 69–114.
- Yang, F., Forrer, P., Dauter, Z., Conway, J.F., Cheng, N., Cerritelli, M.E., Steven, A.C., Pluckthun, A., and Wlodawer, A. (2000). Novel fold and capsid-binding properties of the lambda-phage display platform protein gpD. *Nat. Struct. Biol.* **7**, 230–237.
- Young, R.A., and Davis, R.W. (1983). Efficient isolation of genes by using antibody probes. *Proc. Natl. Acad. Sci. USA* **80**, 1194–1198.